Computational Modelling of Structure and Catalytic Properties of Silica-Supported Group VI Transition Metal Oxide Species

Jarosław Handzlik

Abstract Chromium, molybdenum and tungsten oxides supported on amorphous silica are catalysts for many reactions, including large-scale industrial processes. Although these systems have been extensively studied for many years, there are still a few unresolved issues, concerning mainly the nature of the active sites and mechanisms of their formation. Computational studies, using cluster or periodic models to represent the catalyst surface, are helpful in interpretation of spectroscopic data and can provide complementary information about the catalytic process. In this chapter, such computational works on CrO_x/SiO_2, MoO_x/SiO_2 and WO_x/SiO_2 systems are presented. It is seen that coordination environment of the transition metal, determined also by local surface properties, is a key factor influencing catalytic activity of the surface metal species. This results in complex structure–activity relationships. While a great progress has been achieved in modelling of these systems, from simple clusters to advanced periodic slabs, theoretical determination of complex reaction mechanisms using surface models with representative distribution of metal sites is still a challenge for computational catalysis.

1 Introduction

Group VI transition metal oxides supported on amorphous silica are effective catalysts for many important reactions, including large-scale industrial processes like ethene polymerization or alkene metathesis. These ill-defined systems have been extensively studied for many years using both experimental and theoretical methods. Nevertheless, the structure of the surface chromium, molybdenum and tungsten oxide species on silica has been a subject under debate for a long time, and sometimes contradictory conclusions, based on spectroscopic data, were drawn. Moreover, the nature of the active sites, usually surface organometallic species, as well as the way

J. Handzlik (✉)
Faculty of Chemical Engineering and Technology, Cracow University of Technology,
ul. Warszawska 24, 31-155 Kraków, Poland
e-mail: jhandz@pk.edu.pl

how they are formed, is even less understood. On the other hand, knowledge about the catalyst structure at the atomic level is extremely important for studying the catalytic reaction mechanisms and necessary in effective designing of new catalysts. Coordination environment of the transition metal is a key factor influencing the catalytic properties of the surface metal species. Especially, the local properties of the support, which can be considered as a multidentate ligand coordinated by the metal centre, can dramatically affect the reactivity. However, establishing the structure–activity relationships for silica-supported metal oxide catalysts is still a challenging task, mainly due to heterogeneity of the metal species on amorphous surface and low fraction of the active sites formed in situ.

Computational modelling, taking advantage of growing computer power, enables for development of advanced models representing surface metal species. Density functional theory (DFT) methods, offering a good balance between the accuracy and the cost, are nowadays commonly used in the field of computational catalysis. Theoretical investigations are helpful in interpretation of spectroscopic data concerning supported transition metal oxide species. Quantum chemistry methods, especially when combined with advanced models of the surface, can also provide complementary information about the catalytic system, not accessible at this moment by experimental techniques. Better understanding the nature of the active sites and their precursors, as well as mechanisms of the catalytic reactions and the role of the amorphous surface, is possible owing to computations. Many examples of such computational studies, concerning silica-supported chromium, molybdenum and tungsten oxide systems, are presented in this chapter.

2   Surface Modelling

An adequate model representing surface is crucial for realistic description of the supported metal oxide systems. Especially, modelling amorphous materials with inhomogeneous distribution of surface metal sites is challenging. There are two main approaches to simulate surface of solid, cluster approximation [1–6] and periodic slab models [1–5, 7–10]. A cluster model is a finite fragment cut off from the solid, with dangling bonds usually saturated by hydrogen atoms. Consequently, long-range interactions are neglected, which can be justified for covalent amorphous materials like silica. Small clusters, often used in the past due to limitations of computer power, cannot reproduce the complexity of the amorphous surface, although they are handy for efficient computations of reaction mechanisms. Nowadays, it is possible to employ very big cluster models, containing dozens or even hundreds of atoms [3, 4]. To reduce the computational cost or enlarge the model, partitioning into layers treated at different levels of theory can be done [11]. The active site and its close vicinity are then calculated at a higher level of theory (*inner layer*), while the rest of the system (*outer layer*) is described by a computationally less demanding method. An example of such hybrid method is the ONIOM partitioning scheme [11] (Fig. 1).
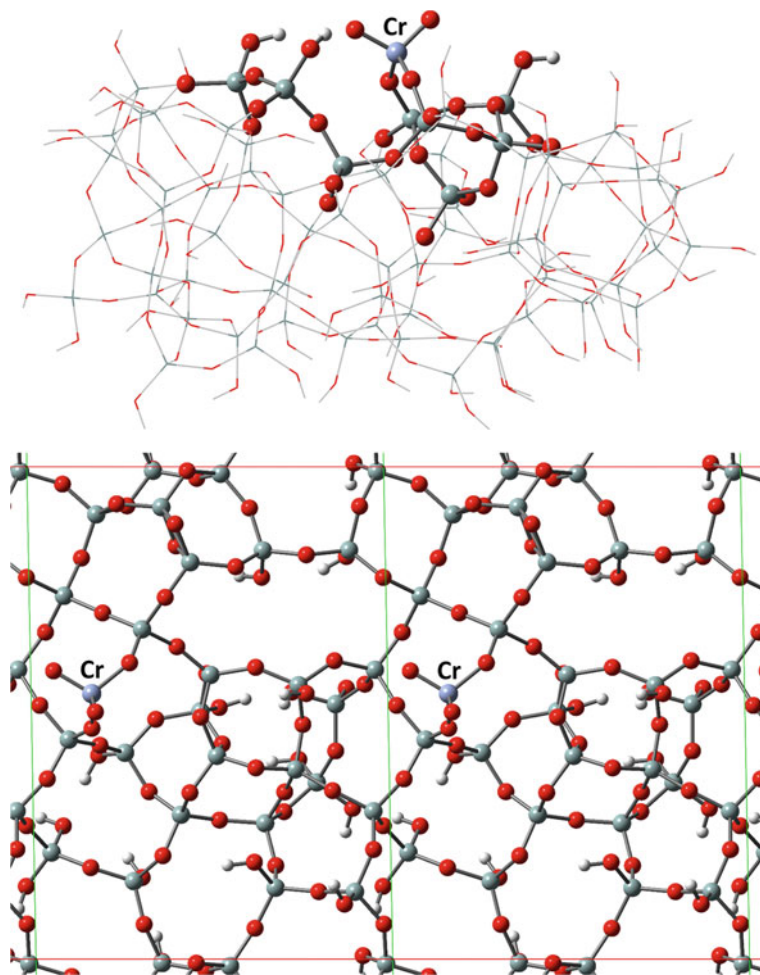
Fig. 1 Example cluster (top) and periodic [4] (bottom) models of Cr(VI) oxide species on silica. In the first case, the two-layer ONIOM method is applied (the wireframe part of the model represents the outer layer)

In the case of the periodic models, the surface of the solid is represented by a slab inside the unit cell that is repeated using periodic boundary conditions (Fig. 1) [1]. For realistic description of the catalyst surface, especially for amorphous materials, the unit cell should be large enough to avoid artificial periodicity and lateral interactions between a surface metal site or adsorbed reactant and its periodic images. Several advanced slab models of amorphous silica were developed from DFT calculations [12–16], and some of them were used in computational studies presented below.

3 CrO$_x$/SiO$_2$ System

Chromia–silica system is well known as the Phillips catalyst for ethene polymerization, discovered in 1950s [17–20]. Approximately 40–50% of the worldwide production of high-density polyethylene is related to this catalyst [17]. A unique property of the Phillips catalyst is the fact that no cocatalyst is necessary to achieve the catalytic activity, in contrast to other transition metal systems used for ethene polymerization, such as Ziegler–Natta and metallocene catalysts. Silica-supported chromium oxide systems are also effective in other catalytic reactions, like dehydrogenation of alkanes [21], oxidative dehydrogenation of hydrocarbons in presence of oxygen [22, 23] or carbon dioxide [24, 25], and various selective oxidation reactions [20, 26–28].

3.1 Structure of Surface Chromium Oxide Species—Experimental Data

Many techniques, including UV-vis, Raman, XANES (X-ray absorption near-edge structure), EXAFS (extended X-ray absorption fine structure), EPR (electron paramagnetic resonance), XPS (X-ray photoelectron spectroscopy) and IR (infrared) spectroscopy, have been used to characterize chromium oxide species on silica. After high-temperature calcination of chromia–silica systems, well-dispersed surface Cr(VI) oxide species are mainly present [17–26, 28–36], although small amounts of Cr(V) and Cr(III) species were also detected, as well as Cr$_2$O$_3$ clusters at higher Cr loadings [17, 19–24, 26, 32, 34]. The nature of the Cr(VI) species on silica has been discussed for many years. Monomeric, dimeric and polymeric Cr(VI) species were often postulated, mainly based on the UV-vis DRS (diffuse reflectance spectroscopy) data [19, 20, 24]. On the other hand, Raman spectroscopy, UV-vis, XANES and EXAFS studies conclusively demonstrated that the monomeric form is the major or even the only surface Cr(VI) oxide species [19, 23, 26, 29–36]. It is described as a tetrahedral dioxo species with two Cr–O–Si linkages (Fig. 2a). Minor five-coordinate monooxo Cr(VI) species, bonded to the silica surface by four Cr–O–Si linkages (Fig. 2b), was also suggested [32–34]; however, this proposal has been recently questioned [35, 36].

Even more complex and problematic is nature of reduced chromium species, which seems to be strongly dependent on the reduction conditions. If CO is used as the reducing agent, Cr(VI) species are almost selectively converted to Cr(II) [5, 17–20, 30, 37–39], whereas reduction with H$_2$ results in Cr(III) [34, 37] or both Cr(III) and Cr(II) [5, 24] oxidation states. The presence of water during reduction favours formation of Cr(III) species [5]. When the calcinated Phillips catalyst is contacted with ethene, Cr(VI) is reduced to Cr(II) and/or Cr(III) [17–19, 34, 40, 41].

According to the UV-vis DRS studies, there are three distinct reduced chromium oxide species on silica: pseudo-tetrahedral Cr(II), pseudo-octahedral Cr(II) and pseudo-octahedral Cr(III) [20, 24, 42]. In addition to the surface reduced chromium

Fig. 2 Proposed structures for monomeric Cr(VI) oxide species on silica
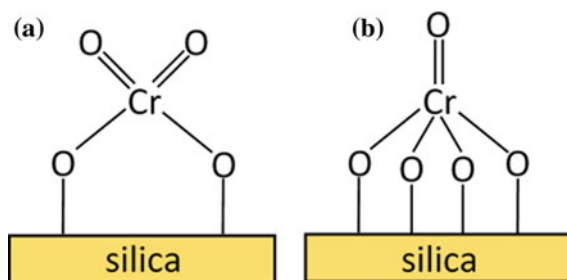
species, Cr_2O_3 clusters can be present [5, 20, 24]. Cr(III) and Cr(II) oxidation states were also detected by XPS [19, 28, 43]. Based on IR spectroscopy data concerning CO chemisorption on the silica-supported Cr(II) species, three families of the Cr(II) sites can be distinguished, characterized by a different degree of coordinative unsaturation [19, 20, 30, 44]. Isolated Cr(V) species, dispersed Cr(III) species and Cr(III) clusters in the CrO_x/SiO_2 systems can be observed by EPR [20, 23, 24, 39, 45–47]. Although intermediate Cr(IV) oxidation state might be also expected during the reduction of the surface Cr(VI) species with two-electron reducing agents, like CO or H_2, there are very few reports suggesting that Cr(IV) species are indeed experimentally observed [38, 39].

3.2 Structure of Surface Chromium Species—Computational Modelling

Taking into account a complex molecular picture of the CrO_x/SiO_2 catalyst and amorphous character of the silica support, computational modelling of this system is a difficult task even today. In the past, only small cluster models of the chromium species on silica were possible to apply for efficient computations. Nevertheless, even simple models, if reasonable constructed, can be helpful in interpretation of spectroscopic data.

Espelid and Børve [48] used F-terminated clusters containing 2–3 Si atoms to calculate d–d transition energies and intensities for monomeric Cr(II) and Cr(III) species, and dimeric Cr(II) species. The transition energies, computed from second-order, multireference many-body perturbation theory (CASPT2 method), were in agreement with the experimental UV-vis DRS data reported for reduced chromia–silica systems. On this basis, the assignment of the experimental bands to specific coordination and oxidation states of chromium was proposed. Mainly the same cluster models were applied to investigate at the DFT level the structure, stability and vibrational properties of surface Cr(II) and Cr(III) species after CO adsorption [49]. Damin et al. [50] computationally studied interaction between Cr(II) species on silica and probe molecules (CO, N_2) employing the model of Espelid and Børve.
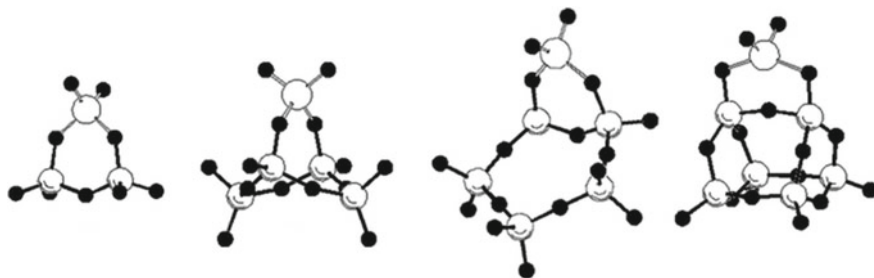
Fig. 3 Cluster models of monomeric dioxo Cr(VI) species on silica. Adapted from [29] with permission from the PCCP Owner Societies

In addition to F-termination of the cluster, other terminations (H, OH) were also examined. Interestingly, by varying the percentage of Hartree–Fock exchange in hybrid DFT functionals, they found that its increase to 35–40% allows for a better agreement with the experimental IR data, compared to the B3LYP method (20% of Hartree–Fock exchange).

In combined experimental and theoretical (B3LYP) studies, Dines and Inglis [29] used cluster models ranging in complexity (Fig. 3) to obtain geometrical parameters of the monomeric dioxo Cr(VI) species on silica and enable the assignment of the measured Raman spectra. It was concluded that only monomeric chromium species are present in the $Cr(VI)/SiO_2$ system at low Cr loading. Recently, the electronic structure of isolated Cr(VI) species on silica was comprehensively investigated using two complementary techniques: UV-vis absorption and fluorescence spectroscopy [35]. The observed electronic absorption spectrum was compared with simulated spectra obtained from TD-DFT (B3LYP) calculations for cluster models of the dioxo Cr(VI) species containing various chromasiloxane ring structures, built based on the models used by Dines and Inglis. Additionally, the five-coordinate monooxo Cr(VI) species was considered. The obtained results provided no evidence for the presence of the monooxo Cr(VI) sites in significant amounts.

Small clusters were also applied to model surface Cr(VI) species which were formed after CrO_2Cl_2 grafting on silica and characterized with IR, XANES and EXAFS spectroscopy [51, 52]. The energetic effects for possible routes for the formation of the surface Cr(VI) sites were calculated with the B3LYP functional. It was concluded that fraction of Cr(VI) species with strained chromasiloxane ring depends on silica dehydroxylation temperature and is related to the catalytic activity in ethene polymerization. In next combined experimental and computational work on this system [53], reduced surface Cr(II) species were modelled by a chromasiloxane ring embedded in a large cluster (37 Si atoms) cut off from the β-cristobalite structure. The ONIOM method and hybrid B3PW91 functional with increased percentage of Hartree–Fock exchange (40%) were used to study adsorption of CO on the Cr(II) sites. They were coordinated by either one or two siloxane ligands, in agreement with EXAFS results. The former, three-coordinate Cr(II) species were proposed to
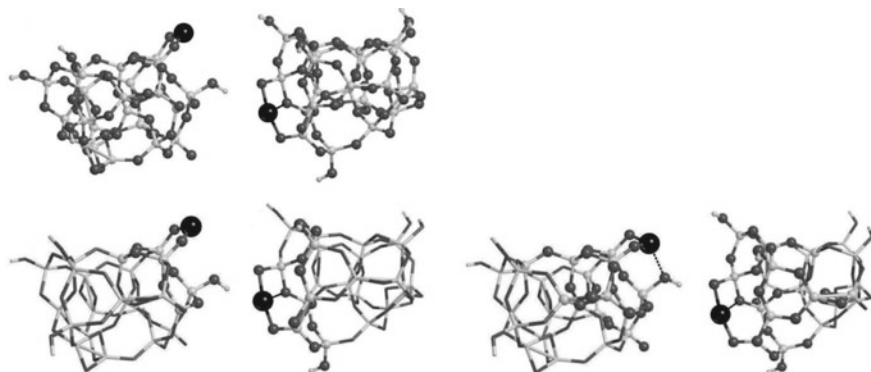
Fig. 4 Cluster models of monomeric Cr(II) species on silica (black sphere: Cr atom). For models at the bottom the ONIOM scheme with differently defined inner layer was applied. Adapted from [44], Copyright (2015), with permission from Elsevier

be relevant for ethene polymerization activity. Based on these results, smaller cluster models of Cr(II) monocarbonyl, Cr(II) dicarbonyl and Cr(III) vinyl species were further built and used in DFT calculations to aid in vibrational assignments in recent experimental studies on the initiation mechanism for the Phillips ethene polymerization catalyst [39, 47].

The ONIOM partitioning scheme was applied for clusters containing 22 Si atoms to model Cr(II) species in the Phillips catalyst (Fig. 4) and examine CO adsorption on these sites [44]. High-level calculations were performed with the long-range corrected hybrid ωB97X-D functional, including empirical dispersion corrections. Additionally, electronic transitions were computed at the TD-DFT level for smaller models, limited to the inner layer. Two differently located Cr(II) sites were modelled. The first one is more coordinatively unsaturated and leads to stable dicarbonyl species upon CO adsorption. In the second one, chromium strongly interacts with a siloxane bridge and monocarbonyl species is rather formed. The models were validated by comparison of the computational results with the experimental IR and UV-vis spectroscopy data for the Cr(II)/SiO$_2$ catalyst with a very low Cr loading. It was concluded that both kinds of the Cr(II) sites coexist in the real system and their relative ratio depends on the activation temperature. Similar computational approach was recently used for modelling Cr(VI) and Cr(II) species on silica and was validated by comparison of the simulated and experimental XANES spectra [41]. Simulation of the XANES spectrum for a model of Cr(II) species with methylformate and two ethene molecules in the coordination sphere supported the proposal based on operando spectroscopic investigations of the Phillips catalyst that sixfold coordinated Cr(II) sites, in interaction with the oxygenated by-products, are mainly involved in ethene polymerization.

Isolated monooxo and dioxo Cr(VI) species on silica under dehydrated conditions were modelled using medium-size (15 Si atoms) clusters derived from the β-cristobalite structure [54]. Geometries of the whole systems were fully optimized

with the PW91 and TPSS functionals to account for the amorphous nature of silica. On the basis of test calculations, the PW91 method was found to be most accurate, among many density functionals, in predicting relative energies of chromium oxo compounds. It was concluded that the relative stability of the monooxo Cr(VI) species, compared to the dioxo one, is much lower than the relative stability of the monooxo Mo(VI) species in the molybdena–silica system, which was earlier computationally studied using analogous models [55].

High-resolution ^{1}H MAS NMR and ^{29}Si CP/MAS NMR spectroscopy was combined with DFT (B3LYP) computations employing polyhedral oligomeric silsesquioxane (POSS) models to investigate the role of various silanol groups in formation of surface Cr(VI) species [56]. It was suggested that monomeric dioxo Cr(VI) species are most favourable located on pairs of a single and an adjacent geminal silanols accompanied with a geminal silanol left. Replacing a pair of geminal silanols by the chromium species is not preferred energetically. The calculated enthalpies of the grafting reactions indicate also higher preference for monomeric Cr(VI) species, compared to Cr(VI) dimers.

Although cluster models of various complexity, representing CrO_x/SiO_2 catalyst, were successfully applied in many computational works, especially those combined with spectroscopic studies, they are usually more or less arbitrarily constructed. To develop more advanced models, being able to reproduce heterogeneity of the surface chromium oxide species, realistic and well-validated models of amorphous silica [12–16] are necessary. Such a model, developed and validated by Tielens et al. [13], representing hydroxylated surface (5.8 OH nm^{-2}) in the unit cell including 120 atoms ($Si_{27}O_{54} \cdot 13\ H_2O$), was employed in systematic computational studies of the Cr(VI)/SiO_2 system [7]. Mono-, di-, tri- and tetragrafted monomeric chromium(VI) species at different degrees of hydration were modelled (Fig. 5). Their formation can be regarded as grafting H_2CrO_4 unit with dehydroxylation of surface silanols. Different types of silanols were involved in grafting reactions: isolated (Si–OH), vicinal (HO–Si–O–Si–OH), geminal (HO–Si–OH) and nonvicinal (two Si–OH groups not directly connected). The relative stabilities of the surface chromium species in a wide range of temperatures were determined from the atomistic thermodynamic approach, based on the calculated energies (PBE functional) for grafting reactions. The monografted hydroxy dioxo Cr species was predicted to be most stable at lower temperatures. An increase of temperature favours digrafted dioxo Cr species (Fig. 2a) and then tetragrafted monooxo Cr species (Fig. 2b). The comparison of the calculated Cr=O stretching frequencies for the surface chromium species with experimental Raman spectra indicated the digrafted dioxo Cr species as the most representative for the Cr(VI)/SiO_2 system.

A large number of periodic and cluster models of the SiO_2 surface were applied in extensive DFT (PW91) investigations of chromium(VI) oxide species on partly dehydroxylated silica [4]. The periodic model of Tielens et al. [7, 13] was properly modified to achieve the initial surface with 3.1 OH nm^{-2}, and, 2.4–1.3 OH nm^{-2} after grafting the Cr species, which roughly corresponds to the conditions of the catalyst thermal treatment before the reaction [17–19, 30, 57, 58]. Similar to the original model, the chromium coverage was about 0.4 atoms nm^{-2}, in agreement
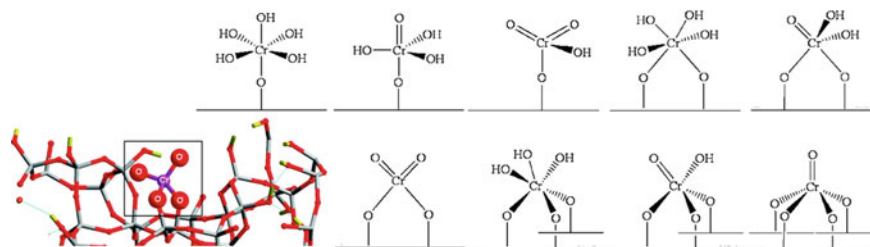
Fig. 5 Modelled Cr(VI) oxide species on hydroxylated silica surface and periodic model of digrafted dioxo Cr(VI) species. Adapted with permission from [7]. Copyright (2012) American Chemical Society

with typical Cr loadings for the Phillips catalyst [17–19, 30]. Based on the periodic models, a set of cluster models (33 Si atoms) was also built. Additionally, cluster models (21, 24, 26 and 72 Si atoms) derived from another structure of amorphous silica were developed, as well as periodic (24 Si atoms in the unit cell) and cluster (63 and 97 Si atoms) models based on the β-cristobalite structure (Fig. 6). With a variety of models, relative stabilities of the tetrahedral dioxo Cr(VI) species and five-coordinate monooxo Cr(VI) species (Fig. 2) were determined. The relative energies were shown to depend on the location of the Cr site on the surface and the structure of the model. More flexible amorphous models allow for easier formation of the four Cr–O–Si linkages of the monooxo Cr(VI) species, compared to the models based on the crystalline structure. Nevertheless, all the approaches led to the same general conclusion that the dioxo Cr(VI) species are more stable than the monooxo species. This is consistent with the above-mentioned experimental results [35, 36]. It was again noticed that the energetic preference for the dioxo Cr(VI) species over the monooxo Cr(VI) species is stronger than in the case of the analogous models for the Mo(VI) species on silica [3]. The vibrational frequency analysis for the variously modelled surface Cr(VI) species, including simulation of the isotopic effect, allowed for a detailed interpretation of the experimental Raman spectra for the Cr(VI)/SiO$_2$ system [4]. It was predicted that the asymmetric O=Cr=O stretching mode for the dioxo species and the Cr=O stretching mode for the monooxo species can overlap.

By considering in the next computational studies [5] dimeric Cr(VI) species on silica, often postulated in the literature [19, 20, 24, 42], it was predicted that they are less stable than the monomeric Cr(VI) species. The structures of various reduced chromium oxide species, both monomeric (Fig. 7) and dimeric (Fig. 8), were also calculated. The use of advanced periodic and cluster models of amorphous silica, taken from the previous work [4], allowed to deal with the heterogeneity of variously located reduced Cr species. For instance, three-coordinate Cr(II) species interacting with siloxane ligand, which was proposed to be relevant in ethene polymerization [39, 44, 53], was directly obtained after geometry optimization without any arbitrarily construction of the model. Therefore, such models can be helpful in investigations of structure–activity relationships for the Phillips catalyst. On the basis of the vibrational frequency analysis, some new assignments for reported Raman spectroscopy data
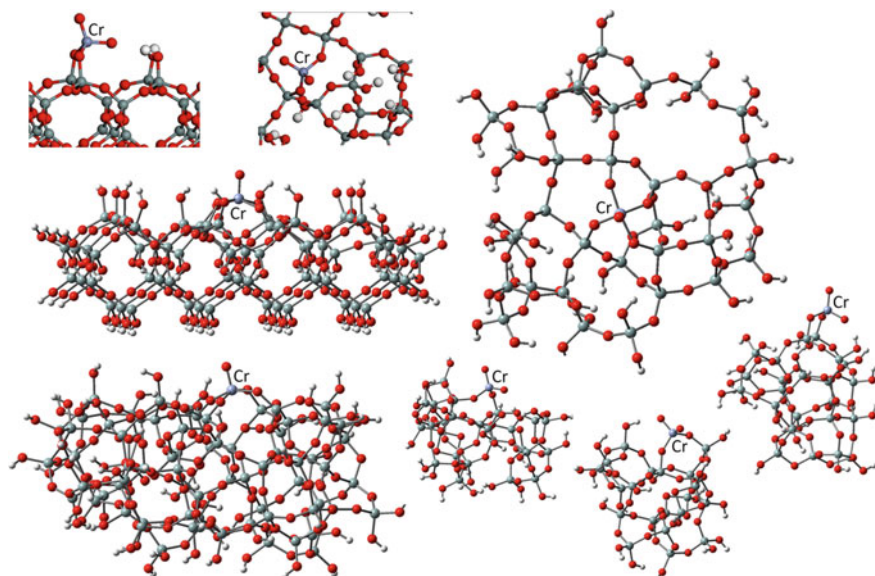
Fig. 6 Example periodic and cluster models of monomeric Cr(VI) oxide species on silica. Adapted with permission from [4]. Copyright (2013) American Chemical Society
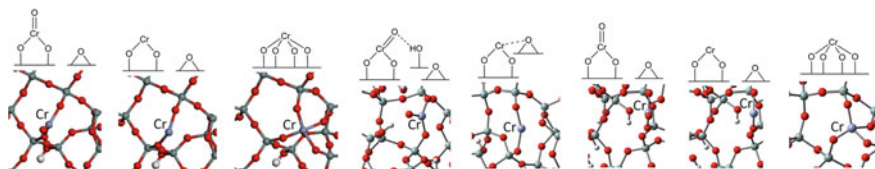
Fig. 7 Example periodic and cluster models of monomeric Cr(IV) and Cr(II) oxide species on silica. Adapted from [5], Copyright (2016), with permission from Elsevier

concerning reduced CrO_x/SiO_2 systems were proposed. The energetic effects of complex redox paths, leading to various Cr(II) and Cr(III) sites, were computed using the PW91 functional. In addition to the DFT calculations, in situ UV-vis DRS studies of the reduction of CrO_x/SBA-1 system with CO and H_2 were carried out. It was observed that the presence of water favours the formation of Cr(III) species, what can be explained, in accordance with the DFT results, by reoxidation of Cr(II) species and hydrolysis of the Cr–O–Si bonds, finally leading to Cr_2O_3 generation. Using the TD-DFT (ωB97X-D) approach, excitation energies for the surface Cr species were calculated. For a given oxidation state of chromium, they depend significantly on the structure of the Cr species and its interaction with the surface siloxane bridges and silanol groups.
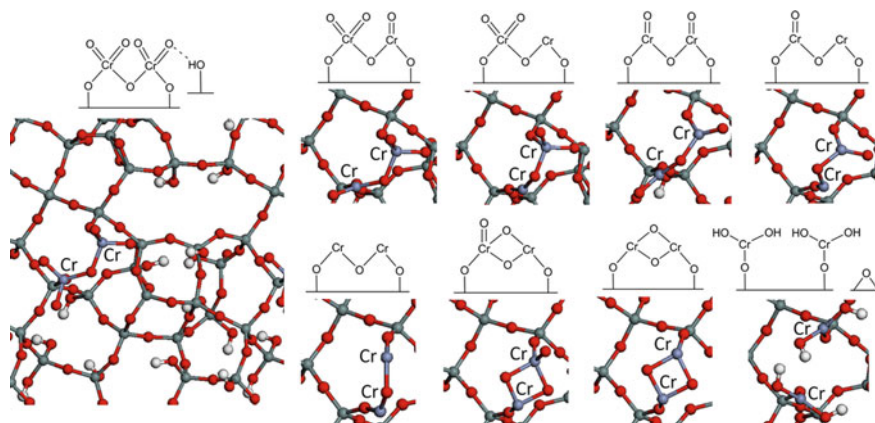
Fig. 8 Example periodic models of dimeric chromium oxide species on silica. Adapted from [5], Copyright (2016), with permission from Elsevier

3.3 Catalytic Activity—Computational Studies

Many theoretical investigations addressed mechanisms of the reactions catalysed by the CrO_x/SiO_2 system. The size of the models was usually limited to reduce computational cost of exploring many potential reaction pathways. In DFT (BP86) studies of ethane dehydrogenation over Cr(III) sites on silica, cluster models constructed either in ad hoc manner or systematically, starting from low-index surfaces of α- and β-cristobalite, were used [59, 60]. To examine the accuracy of the cluster approximation, hybrid QM/MM periodic calculations were also done. Mechanism of acetylene and methylacetylene cyclotrimerization catalysed by $Cr(II)/SiO_2$ system was investigated with a simple cluster model (2 Si atoms) representing chromasiloxane ring [61, 62]. On the basis of benchmark calculations of triplet–quintet energy gaps performed for many density functionals, taking the CASPT2 value as the reference, the B3PW91 functional with Hartree–Fock exchange increased to 28% was selected for the mechanistic calculations [61].

Despite many decades of investigations, the nature of the active sites in the Phillips catalyst, as well as the mechanism of their formation, is still not well recognized and raise much controversy in the literature. CrO_x/SiO_2 does not require any cocatalyst as a source of alkyl group to form the polymer chain via the Cossee–Arlman insertion. Instead, ethene must somehow react with surface chromium species to generate the initiating ligand. A lot of computational works concerning the CrO_x/SiO_2 system were focused on this issue.

First comprehensive computational studies on the mechanism of ethene polymerization over the Phillips catalyst were performed by Espelid and Børve [63–65]. They compared several initiation and propagation routes using the BP86 functional and small cluster models representing monomeric and dimeric reduced chromium species on silica. It was concluded that various chromium(IV) organic species, being potential

products of reaction between monomeric Cr(II) site and ethene, are not effective in chain propagation [63]. However, easily generated Cr(IV) chromacyclopentane intermediate can lead, after ethylene insertion, to experimentally observed [66] 1-hexene formation. The latter is a product of intramolecular β-H transfer, which competes with the ring expansion, and the kinetic preference depends on the Cr site strain. On the other hand, Cr(III) alkyl site was predicted to be the active propagating species, although the mechanism of its formation was not explained [63]. Instead, generation of propagating Cr(IV) alkyl site through hydrogen transfer from a surface silanol to Cr(II) species was later proposed [64]. Another initiation route postulated involves dimeric Cr(II) species which might react with ethene to form cyclic dimeric Cr(III) propagating species without external sources of hydrogen [65].

Various initiation pathways for the Phillips catalyst, starting from Cr(II) site modelled by chromasiloxane ring (2 Si atoms), were calculated with the B3LYP functional [67]. The key intermediate was Cr(IV) chromacyclopentane species. According to their experimental results [43, 68], the authors took into account the presence of formaldehyde, which can be formed during reduction of the surface Cr(VI) species by ethene. They found that adsorption of one formaldehyde molecule on the Cr site favours ethene dimerization to 1-butene through Cr(IV) hydride intermediate and metathesis to form propene/ethene through a Cr(IV) chromacyclobutane intermediate. This proposal might explain experimentally observed production of propene and butene during the induction period of ethene polymerization over the Phillips catalyst [43, 68]. On the other hand, after formaldehyde desorption, a ring expansion pathway to Cr(IV) chromacycloheptane and subsequent one-step reductive elimination of 1-hexene were predicted to be kinetically preferred.

Conley et al. [69, 70] showed that well-defined Cr(III)/SiO$_2$ catalysts are active in ethene polymerization. They proposed that heterolytic C–H bond activation of ethene forms the first Cr–C bond, which was supported by computational (B3LYP-D3) studies [70]. Two F-terminated cluster models were constructed (Fig. 9), representing major tri-coordinate Cr(III) species and minor species with Cr(III) coordinated to an additional siloxane bridge, which was confirmed by comparison of experimental and computed vibrational shifts after CO adsorption. The calculated reaction pathways included initiation by hydrogen transfer from ethene to generate (≡SiO)$_2$(≡SiOH)Cr(III)-vinyl species, subsequent propagation according to the Cossee–Arlman mechanism and less kinetically favoured termination via reverse hydrogen transfer to chromium alkyl. Coordination of two ethene molecules to the Cr(III) site facilitates the C–H bond activation, but it is prevented if the additional siloxane ligand is present. On this basis, it was suggested that Cr(III) sites coordinating siloxane bridge are inactive in polymerization. The same computational approach was used for investigations of propane dehydrogenation over the Cr(III)/SiO$_2$ system [70].

The C–H bond activation mechanism was further re-examined by Fong et al. [6], who used the same cluster model representing Cr(III) species and concluded that the initiation step is too slow. In addition, they found a termination route which is faster than propagation, so only oligomers would be formed. Similar results were obtained for the analogous mechanism on Cr(II) site represented by the chromasiloxane cluster
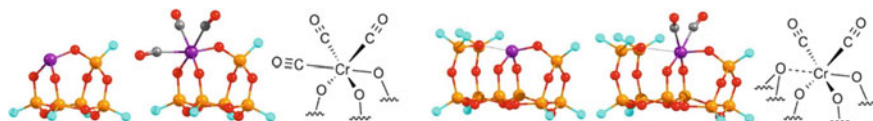
Fig. 9 Cluster models of Cr(III) oxide species on silica and the corresponding CO adducts. Adapted with permission from [70]. Copyright (2015) American Chemical Society

(2 Si atoms). Other routes considered for the Cr(II) site, i.e., chromacycle ring expansion, oxachromacycle ring expansion and carbene mechanism, were also excluded because of too high Gibbs energy barriers calculated (ωB97X-D functional) for the initiation or propagation steps. Instead, ($\equiv$SiO)$_2$Cr(III)-alkyl species without vinyl end were proposed as the active sites; however, the mechanism of their formation remained unknown.

A large number of potential initiation (Fig. 10), propagation and termination mechanisms for ethene polymerization involving surface Cr(II), Cr(III) and Cr(V) sites on silica were computationally investigated on the PBE0-D3 level [71], applying cluster models obtained from the β-cristobalite or amorphous silica [4, 13] structure (Fig. 11). It was predicted that Cr(II) oxachromacycle ring expansion is a more effective polymerization mechanism than the routes via Cr(II) chromacycle or ($\equiv$SiO)($\equiv$SiOH)Cr(II)-vinyl site, mainly because of the kinetic preference for propagation, compared to the termination step. The mechanisms involving Cr(III) oxachromacycle [40, 71] or ($\equiv$SiO)$_2$($\equiv$SiOH)Cr(III)-vinyl species would be less kinetically accessible than the corresponding routes for the Cr(II) sites. However, the calculated barriers might strongly depend on a silica model used, i.e. on a more realistic description of the local coordination environment. It was also shown that ($\equiv$SiO)$_2$Cr(III)-OH species can transform into ($\equiv$SiO)$_2$Cr(III)-CH=CH$_2$ [40, 71], which enables rapid propagation, kinetically favoured over the possible termination steps. The proposed mechanism was consistent with operando spectroscopy studies [40], which indicated the Cr(III) vinyl site as the active reaction intermediate during ethylene polymerization over the CrO$_x$/SiO$_2$ catalyst. Trying to explain how Cr(III) sites might be generated from Cr(II) species, most likely formed in the Phillips catalyst after Cr(VI) reduction by ethene, it was suggested that defect sites on the silica surface can play a role [71].

Structure–activity relationships for well-defined Cr(III)/SiO$_2$ catalyst were studied with periodic DFT (PBE) approach [10], based on the amorphous silica model [15] with 372 atoms in the unit cell and a surface silanol density of 1.1 OH nm^{-2}. The models of surface Cr(III) species were constructed by substituting $\equiv$SiOH fragments with Cr (Fig. 12). Reactivity of five resulting ($\equiv$SiO)$_3$Cr(III) sites of different location and strain were compared for the C–H bond activation and oxachromacycle ring expansion mechanisms. It was found that both routes are facilitated by strained Cr(III) species and propagation is more accessible kinetically than termination. Strained sites favour the oxachromacycle pathway of ethene polymerization, whereas both mechanisms can compete in the case of less strained and thereby less
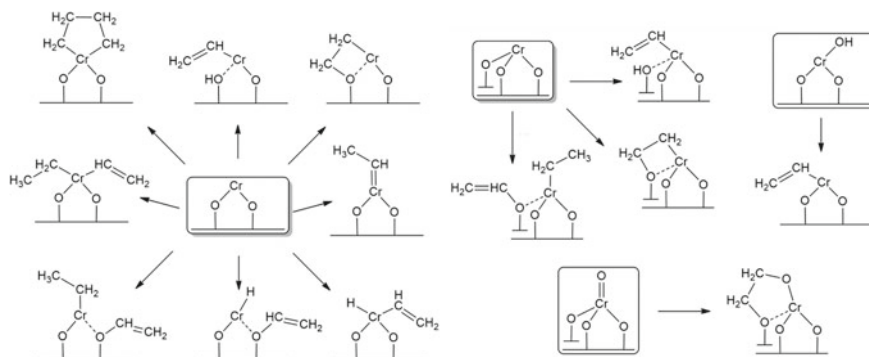
Fig. 10 Potential initiation routes for ethene polymerization involving Cr(II), Cr(III) and Cr(V) oxide species on silica. Adapted from [71], Copyright (2017), with permission from Elsevier
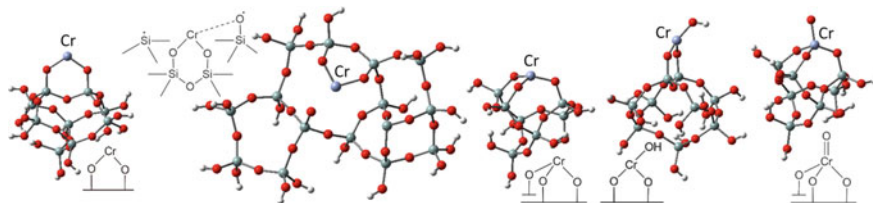
Fig. 11 Cluster models of Cr(II), Cr(III) and Cr(V) oxide species on silica. Adapted from [71], Copyright (2017), with permission from Elsevier

active Cr(III) species. On this basis, the authors suggested that the distribution of active sites with different local environments accounts for the broad distribution of polymer chains. In the next work of this group [72], the oxachromacycle ring expansion and C–H bond activation mechanisms were theoretically examined for propene polymerization, which allowed to explain experimentally observed different reactivity of the well-defined Cr(III)/SiO$_2$ system towards ethene and propene.

An influence of the coordination environment of the surface chromium species on their reactivity was also pointed in the next computational work of Fong et al. [73]. By applying cluster models, the ωB97X-D functional and variational transition state theory, they examined a one-electron initiation mechanism for ethene polymerization over the Phillips catalyst, according to Kissin and Brandolini proposal [74]. In the first step, various organo-Cr(IV) sites might be formed by oxidative addition of ethene to surface Cr(II) species. Intramolecular hydrogen transfer in Cr(II) bis(ethene) complex would lead to ($\equiv$SiO)$_2$Cr(IV)(CH$_2$–CH$_3$)(CH=CH$_2$) species. Subsequent Cr–C bond homolysis gives active ($\equiv$SiO)$_2$Cr(III)(CH=CH$_2$) site and ethyl radical, in agreement with the observed generation of organic radicals [47] and Cr(III) vinyl species [40, 47] during the initiation stage of ethene polymerization. The studied effect of siloxane coordination to the Cr site suggested that the proposed mechanism might be effective if the siloxane ligands were hemilabile, allowing
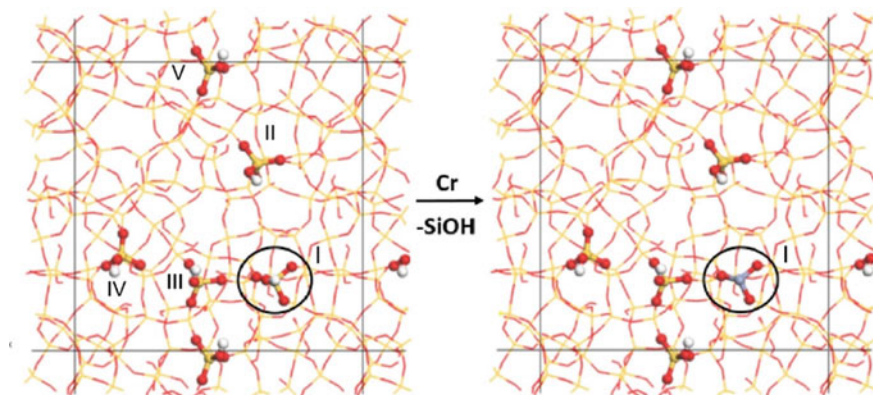
Fig. 12 Construction of Cr(III)/SiO$_2$ periodic model by substitution of one of the five SiOH groups in the unit cell with Cr. Reprinted from [10], Copyright (2017), with permission from Elsevier

access to lower and higher coordination states during the first and second initiation steps, respectively (Fig. 13). However, to confirm such a scenario, a more advanced model would be required, reproducing the flexibility of the silica framework. Because Cr(IV) chromacyclopentane site is the most kinetically accessible product of oxidative addition of ethene to Cr(II), an alternative Cr–C bond homolysis mechanism was examined [75]. According to this proposal, Cr(IV) chromacyclopentane species undergoes homolysis to generate tethered butyl radical which can attach to an adjacent Cr(II) site forming an n-butyl bridge. Then, ethene insertion might occur at both of the resulting Cr(III) alkyl sites. Although this mechanism does not require a change in Cr coordination number during the reaction, it needs neighbouring Cr sites instead.

In most industrial polymerization processes by the Phillips technology, the initial Cr(VI) species are reduced by ethene; however, the reaction mechanisms for the reduction stage are not well recognized. This issue was addressed in computational (PBE0-D3) studies using cluster models developed from the β-cristobalite structure [76]. It was shown that the reduction mechanism strongly depends on the coordination of the surface Cr(VI) sites. In the case of the major four-coordinate dioxo Cr(VI) species, the most kinetically favoured reduction pathway involves both oxo ligands and leads to the formation of Cr(II) site and two formaldehyde molecules. Potential minor five-coordinate monooxo Cr(VI) species would be reduced to a very stable cyclic Cr(IV) site, being rather a spectator species than a reactive intermediate. Reduction of the dioxo and monooxo Cr(VI) species by CO also leads to Cr(II) and Cr(IV) sites, respectively. To explain experimentally observed CO$_2$ release after treating of the Cr(VI)/SiO$_2$ system with ethene at higher temperatures [40], the mechanism of formaldehyde oxidation to carbon oxides and water was proposed. An alternative conversion of formaldehyde to methyl formate over Cr(II) sites, as suggested from experimental investigations [41], was examined too; however, the calculated pathways are less kinetically accessible. On the other hand, transforma-
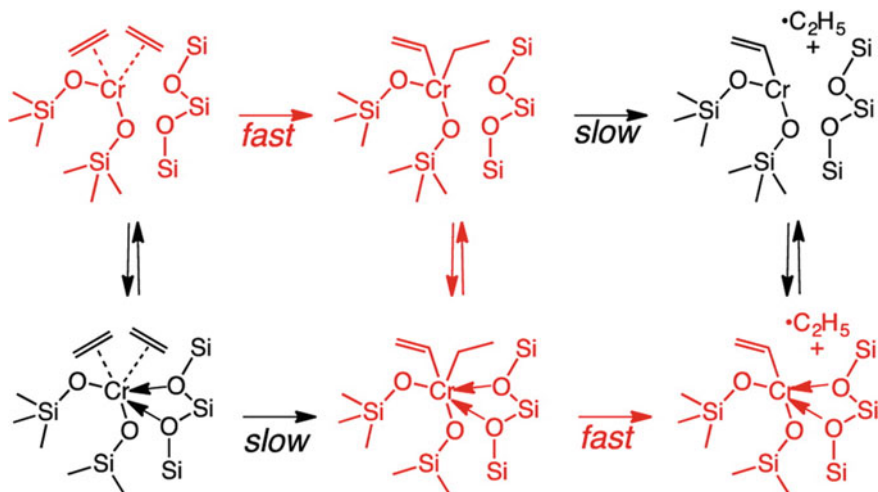
Fig. 13 Proposed initiation mechanism for ethene polymerization over the Phillips catalyst, requiring hemilabile siloxane ligands. Reprinted with permission from [73]. Copyright (2016) American Chemical Society

tion of formaldehyde to various surface intermediates was predicted to occur easily, which might explain why formaldehyde is usually not detected in gas phase during the early stage of ethene polymerization.

4 MoO$_x$/SiO$_2$ System

Molybdenum oxide supported on amorphous silica is a popular catalyst which exhibits activity in a variety of reactions, including alkene metathesis [77–85], selective oxidation of methane [86–88], alkenes [22, 89, 90] and alcohols [27, 91–93], as well as, oxidation of ammonia [94]. The active sites or their precursors are usually highly dispersed surface molybdenum species, often proposed to be monomeric species [78, 81–85, 88].

4.1 Structure of Surface Molybdenum Oxide Species—Experimental Data

The structure of the silica-supported Mo(VI) species under dehydrated conditions have been discussed for many years, on the basis of UV-vis, Raman, XANES, NEX-AFS, EXAFS and IR spectroscopy results [32, 33, 81, 84, 85, 87–90, 92, 95–104]. Today, it is rather established that the isolated surface Mo(VI) sites are present as
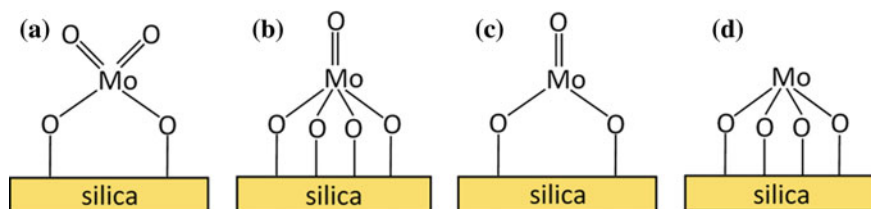
Fig. 14 Proposed structures for monomeric Mo(VI) and Mo(IV) oxide species on silica

major four-coordinate dioxo Mo(VI) species (Fig. 14a) [32, 33, 81, 84, 89, 90, 97, 99–101, 104]. Minor five-coordinate monooxo Mo(VI) species can also exist (Fig. 14b). Some authors also proposed dimeric/oligomeric Mo(VI) oxide species [85, 102, 103] or clusters [85], besides monomers, at relatively low Mo loadings. At higher Mo content, crystalline MoO_3 phase is additionally observed [32, 84, 104].

Considering the reduced MoO_x/SiO_2 catalyst, two or three distinct Mo(V) species on silica were observed with EPR after reduction of the Mo(VI)/SiO$_2$ system by H_2 [79, 105] or its thermal treatment in inert gas [79]. XPS measurements indicated the existence of Mo(VI), Mo(V) and Mo(IV) states after more severe reduction of the catalyst by H_2 [79]. The presence of Mo(IV) species in H_2-reduced MoO_x/SiO_2 system was supported by XANES studies [88, 98]. Effective generation of surface Mo(IV) species by photoreduction of molybdena-silica catalysts in CO was also reported [77, 78]. The nature of the Mo(IV) species might depend on the precursor structure (Fig. 14).

4.2 Structure of Surface Molybdenum Species—Computational Modelling

Similar to modelling chromia–silica catalysts, rather simple cluster models were used in the past to represent molybdenum oxide species on silica. Radhakrishnan et al. [97] combined NEXAFS, EXAFS and Raman spectroscopy studies of the Mo(VI)/SiO$_2$ system with Hartree–Fock calculations using small cluster models (1–2 Si atoms). They found that tetrahedral dioxo and distorted octahedral Mo(VI) species, the latter modelled as five-coordinate monooxo species, can be present on the silica surface. On the basis of DFT (B3LYP) calculations with slightly larger cluster models, Chempath et al. [106] proposed that surface dioxo and monooxo Mo(VI) species (Fig. 14a, b) can be in equilibrium with each other. However, by comparing XANES and EXAFS spectra simulated for the Mo(VI) and Mo(IV) models with the corresponding experimental spectra, they concluded that isolated Mo(VI) sites on silica are present as dioxo species, and Mo(IV) sites exist as three-coordinate monooxo species (Fig. 14c). This proposal was additionally confirmed by vibrational frequency analysis, referred to experimental Raman data at the time. In contrast,
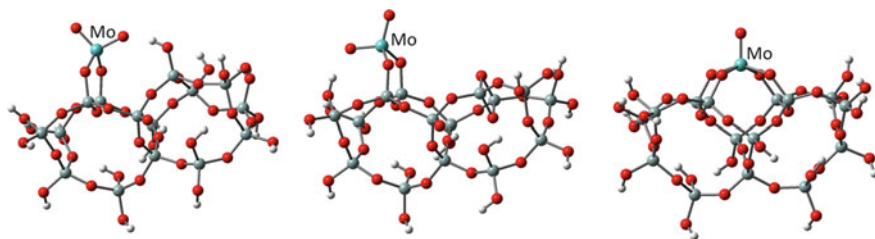
Fig. 15 Cluster models of Mo(VI) oxide species on silica. Adapted from [55], Copyright (2009), with permission from Elsevier

the results of B3LYP cluster studies employing the POSS model to represent silica suggested that the vibrational assignments for the surface Mo(VI) species might be reverse than those originally proposed from the experiment [32, 33] and, therefore, the monooxo Mo(VI) species might be dominant [107]. The POSS-based cluster models were also applied in combined computational (RPBE) and experimental investigations of MoO_x/SBA-15 system [101]. By comparison of the calculated and experimental NEXAFS spectra, it was concluded that the tetrahedral dioxo Mo(VI) species is the major species, while the pentahedrally coordinated monooxo Mo(VI) species exists in small quantities if at all.

Relative energies of the dioxo and monooxo Mo(VI) species on silica, represented by medium-size (15 Si atoms) cluster models (Fig. 15) derived from the β-cristobalite structure, were computed with various density functionals, selected on the basis of test calculations for molybdenum oxo compounds [55]. Although the monooxo species was predicted to be more stable, the theoretically determined Mo=O stretching frequencies confirmed the vibrational assignments [32, 33] indicating that the dioxo species is dominant.

In comprehensive DFT (PW91) studies of the MoO_x/SiO_2 system [3], a variety of advanced cluster models (15–97 Si atoms) were developed from the β-cristobalite and amorphous silica structure (Fig. 16). The two-layer ONIOM partitioning scheme was adopted to the largest models. In addition, periodic models based on the β-cristobalite framework were applied. It was found that relative energies of the Mo(VI) species depend on their location and a silica model used. If the local silica structure is flexible enough to facilitate formation of four Mo–O–Si linkages, the monooxo Mo(VI) species (Fig. 14b) are thermodynamically preferred under dehydrated conditions. Most locations, however, due to geometrical constraints on the surface, are favourable for the dioxo Mo(VI) species (Fig. 14a), which therefore should be in majority. This conclusion was supported by the vibrational frequency analysis, consistent with the proposed assignments of the experimental Raman bands [32, 33]. Reduction of the surface Mo(VI) species to Mo(IV) sites by H_2 was calculated as a highly endergonic process, in contrast to the exergonic reduction of Cr(VI) to Cr(IV) [5], which is in agreement with much worse reducibility of molybdena–silica catalysts, compared to chromia–silica systems. It was predicted that relative stabilities of the Mo(IV) species (Fig. 14c, d) are determined by the relative energies of the corresponding
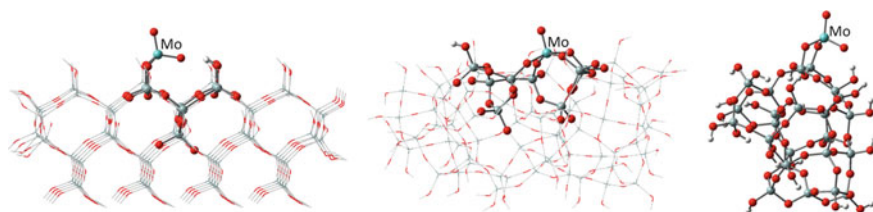
Fig. 16 Example cluster models of Mo(VI) oxide species on silica. In the first two cases, the ONIOM method is applied. Adapted with permission from [3]. Copyright (2012) American Chemical Society

Mo(VI) precursors; hence, three-coordinate monooxo Mo(IV) species (Fig. 14c) are most likely formed during Mo(VI) reduction with two-electron reducing agents.

Dioxo functionality of the major monomeric Mo(VI) species on silica was also confirmed by DFT (PBE) atomistic thermodynamic approach combined with vibrational frequency analysis [8]. Analogous to the previous work on CrO_x/SiO_2 system [7], mono-, di, tri- and tetragrafted monomeric molybdenum(VI) species at different degrees of hydration were considered using the slab model of hydroxylated silica surface [13]. The Mo grafting site was investigated systematically for the type of silanol (isolated, vicinal, geminal, nonvicinal or in a nest) accessible on the surface, as well as its effect on hydrogen bond formation with the Mo species and its stabilization. Based on calculated surface Gibbs energies and comparison between calculated and experimental vibrational frequencies, the digrafted dioxo Mo(VI) species (Fig. 14a) was predicted to be the dominant over a wide range of temperatures. Only at low temperatures, a monografted hydroxy dioxo Mo(VI) species would be more preferred thermodynamically. The tetragrafted monooxo Mo(VI) species (Fig. 14b) is more stable than the digrafted dioxo species, but it requires a nest of at least four silanol groups for grafting, so its presence is merely due to the distribution of the silanol density on the surface. This conclusion is consistent with the postulated geometrical constrains on the dehydroxylated silica surface, which hinder the formation of the tetragrafted monooxo Mo(VI) species [3].

4.3 Catalytic Activity—Computational Studies

Both dioxo and monooxo isolated Mo(VI) species were considered as the active sites or their precursors in computational studies of reactions catalysed by the MoO_x/SiO_2 system. Based on B3LYP cluster calculations, two mechanisms were proposed for methane oxidation to formaldehyde, depending on which Mo(VI) species, the dioxo or monooxo one, is assumed as the active site [108]. It was shown that the pathway involving the dioxo Mo(VI) species and reduced monooxo Mo(IV) species (Fig. 14a, c) is in a better agreement with experimental kinetic data. The mechanisms of methanol oxidation to formaldehyde over the dioxo and monooxo Mo(VI)

sites were also found to be different each other and only in the latter case cleavage of the Mo–O–Si linkage is predicted [107].

Similar to other supported metal oxide catalysts for alkene metathesis, active metal alkylidene sites in the MoO_x/SiO_2 system are generated in situ from the surface Mo oxide species upon contact with alkene [82–85]. Among several initiation mechanisms considered in the literature, reduction of Mo(VI) to Mo(IV) with propene, followed by 1,2-hydrogen shift, was recently proposed, based on experimental results [82, 83]. It was also reported that high-temperature activation of the MoO_x/SiO_2 catalyst under an alkene-containing atmosphere is highly efficient for low-temperature alkene metathesis [85]. However, these issues were not addressed in computational works, although the propagation mechanism for alkene metathesis was studied in detail.

In a series of papers [109–111], DFT (B3LYP) studies of alkene metathesis over MoO_x/SiO_2 catalyst were reported. The Mo(VI) and Mo(IV) alkylidene species (Fig. 17) were represented by various cluster models (7–49 Si atoms) derived from the β-cristobalite structure. The largest models were developed using the two-layer ONIOM partitioning scheme [110, 111]. By exploring the pathways of ethene metathesis over tetrahedral Mo(VI) methylidene sites, it was found that a cycloreversion step, involving trigonal bipyramidal (TBP) molybdacyclobutane intermediate, is more favoured kinetically than a side transformation to a more stable square pyramidal (SP) molybdacyclobutane [109], in contrast to the theoretical results reported for molybdena–alumina systems [112–115]. The TBP → SP pseudorotation was proposed to be a reversible deactivation route. The comparison of the computed and experimental [78] C–H stretching frequencies suggested that the experimentally observed molybdacyclobutane species were the stable SP sites, not the reactive TBP intermediates. It was also shown that metathesis activity of the Mo(VI) alkylidene sites strongly depends on their location on the silica surface, similar to Mo(VI) alkylidene species on γ-alumina [113–116]. The electronic and geometrical structure analysis indicated that the main factor affecting the reactivity is the geometry of the Mo site, determined by surface constrains [109, 111]. Especially, the more advanced models (Fig. 18) enabled investigations of the relationship between metathesis activity of the tetrahedral Mo(VI) methylidene species (Fig. 17a) and the local structure of partially dehydroxylated silica surface [111]. Five-coordinate Mo(VI) alkylidene species (Fig. 17b) and Mo(IV) alkylidene species (Fig. 17c) were also examined, and it was concluded that these sites are inactive in alkene metathesis, in contrast to the four-coordinate Mo(VI) alkylidene sites, further additionally studied with the paired interacting orbitals (PIO) method [117]. Thus, it was shown [109, 111] that the metathesis activity of the Mo alkylidene sites is determined by the coordination environment of molybdenum, its oxidation state and the geometry of the Mo species, which is influenced by the local structure of the silica surface. The latter factor reflects heterogeneity of the active Mo sites.

Another strategy to account for inhomogeneous distribution of active sites on amorphous supports and investigate the structure–reactivity relationship was proposed by Goldsmith et al. [118]. They developed an algorithm which generates a representative set of small cluster models allowing to relate the activation energy
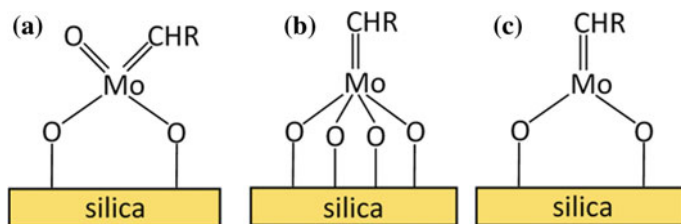
Fig. 17 Potential structures of Mo(VI) and Mo(IV) alkylidene species on silica
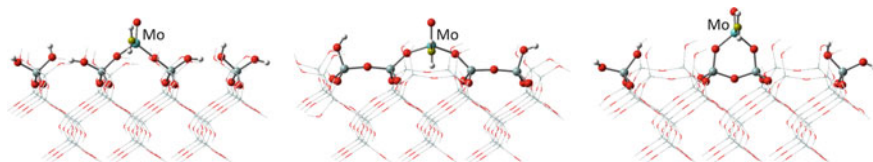
Fig. 18 Example models representing tetrahedral Mo(VI) methylidene species on SiO_2 which differ significantly each other in predicted metathesis activity. Adapted with permission from [111]. Copyright (2007) American Chemical Society

to the geometry and energy of the active site. By applying this method to model the above-mentioned TBP → SP molybdacyclobutane pseudorotation, they found a clear relationship between the Si–Si distance and the activation barrier. The same reaction was later studied by Ewing et al. [119] who used an advanced periodic model of amorphous silica (250–270 atoms in the unit cell) [14], considering 15 different surface structures with silanol density of 4, 3.2 and 2.3 OH nm^{-2}. They developed an approach for generating a large number of isolated metal atom sites on amorphous surface (Fig. 19). It was shown that the local structure of silica in the vicinity of the Mo site affects significantly the reaction and activation energy. A very complex structure–energy relationship was revealed, which results from various effects, including the Mo site interactions with neighbouring silanols and rotation-induced relaxation of the surface, which are not accounted for in small cluster models.

5 WO_x/SiO_2 System

Silica-supported tungsten oxide is mainly used as the industrial catalyst for metathesis of light alkenes [84, 85, 120–123]. In the past, ethene and butene were produced from propene in the Phillips triolefin process. Nowadays, due to a world shortage of propene, the reverse process, known as olefins conversion technology (OCT), is carried out on a large scale. The WO_x/SiO_2 system is also active in other catalytic reactions, including selective oxidation of methane [124], butene [22], styrene [125] and methanol [27], as well as, photocatalytic water splitting [126]. Similar to
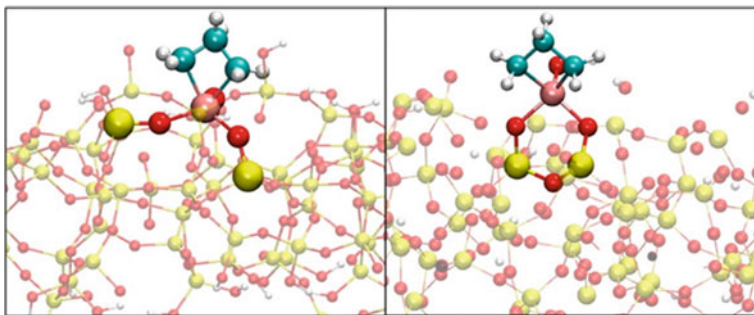
Fig. 19 Example models of SP molybdacyclobutane species differently located on the silica surface. Adapted with permission from [119]. Copyright (2016) American Chemical Society

CrO_x/SiO_2 and MoO_x/SiO_2, the catalytic activity of WO_x/SiO_2 is often attributed to well-dispersed surface metal oxide species [84, 85, 121–123, 126].

The structure of the surface W(VI) species in oxidized WO_x/SiO_2 systems under dehydrated conditions was determined mainly from in situ Raman, UV-vis, XANES and EXAFS studies [32, 33, 84, 100, 121]. It was postulated that isolated four-coordinate dioxo W(VI) species and five-coordinate monooxo W(VI) species coexist on the silica surface and their ratio is a function of temperature. On the other hand, surface oligomeric W(VI) species were sometimes proposed [127, 128]. At higher tungsten loadings, crystalline WO_3 nanoparticles are also present [32, 84, 121, 127, 128].

Following the previous computational works on silica-supported chromium(VI) [7] and molybdenum(VI) [8] oxide species, Guesmi et al. [9] performed DFT (PBE) studies of isolated tungsten(VI) oxide species on hydroxylated silica surface represented by the slab model of Tielens et al. [13]. Thermodynamic stability of mono-, di, tri- and tetragrafted monomeric tungsten(VI) species at different degrees of hydration was determined for a wide range of temperatures (Fig. 20). It was predicted that hydrated species with W–OH groups might be present only at very low temperatures. In more typical conditions, five-coordinate monooxo W(VI) species was found to be most stable; however, this tetragrafted species is statistically disfavoured due to the low probability to have four silanols, required for grafting, in one nest. For this reason, the digrafted dioxo W(VI) species is expected to dominate over the more thermodynamically preferred monooxo species. The presence of both dioxo and monooxo species was additionally confirmed by the computed W=O stretching frequencies, being close to the corresponding experimental Raman data. Finally, a comparison between the tungsten oxide species and other group VI metal oxide species on silica confirmed a greater similarity with the Mo species than with the Cr species.

In recent experimental works [85, 121–123], activation of the WO_x/SiO_2 catalyst for alkene metathesis was extensively investigated. It was postulated that the isolated dioxo W(VI) species are the active site precursors. Similar to the MoO_x/SiO_2 system,
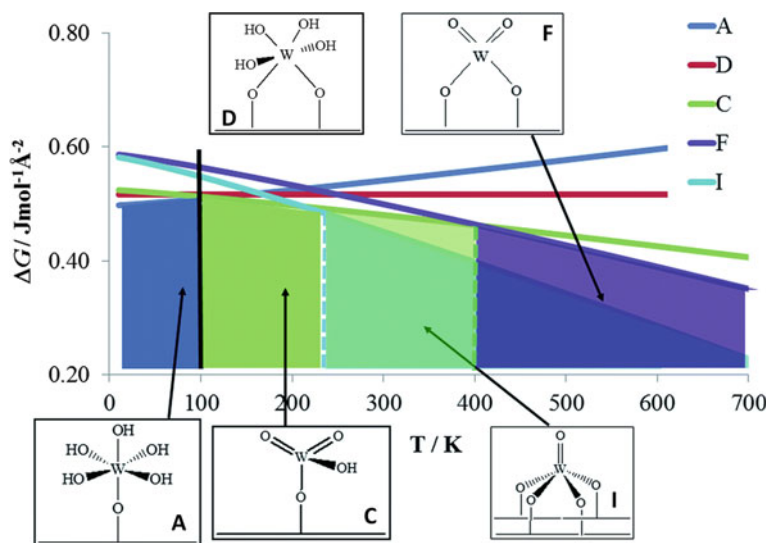
Fig. 20 Phase diagram (surface energy vs. temperature) showing the stability ranges for various W(VI) oxide species on silica [9]—adapted by permission of The Royal Society of Chemistry

the high-temperature activation in the presence of alkene was found to be very effective [85]. It was also proposed that three distinct sites of different metathesis activity are generated during the catalyst activation with alkenes [122]. Surprisingly, computational studies on the mechanism of alkene metathesis catalysed by the WO_x/SiO_2 system were not reported.

6   Concluding Remarks

From the computational works presented in this chapter, it is evident that a great progress has been achieved in the field of modelling silica-supported group VI metal oxide systems. Whereas only simple and more or less arbitrarily constructed cluster models could be used in the past, the most advanced today's slab models contain hundreds of atoms in the unit cell and are able to account for the heterogeneity of the surface metal species.

A number of theoretical works concerned the CrO_x/SiO_2 system, mainly as the Phillips catalyst for ethene polymerization. They addressed the nature of the oxidized and reduced chromium oxide species on silica, as well as polymerization mechanisms, especially formation of the active sites. It seems that the latter subject still requires further investigations, although many new important results, both experimental and theoretical, were reported recently.

Modelling of the molybdenum oxide species on silica allowed to support the experimental proposals about their structure. The MoO_x/SiO_2 system was also computationally studied as the catalyst for selective oxidation reactions and alkene metathesis. However, the still unknown mechanism of generation of the metathesis active sites in this system was not examined, and theoretical studies on this issue would be desired.

Although the WO_x/SiO_2 system is an important industrial catalyst for alkene metathesis, computational works on the metathesis activity of the surface tungsten oxide species on silica are lacking, only the structure of the W(VI) species was modelled. Hence, further theoretical investigations of this system are also needed.

Combined with experimental results, computational studies often enabled for better recognizing of the structure of the surface metal species on silica. On the other hand, many mechanisms of the catalytic reactions, especially the formation of the active sites from the metal oxide precursors, have not been understood well enough yet. Applying advanced surface models with representative distribution of metal sites to determine complex reaction mechanisms and structure–activity relationships seems to be a challenge for future works. Even more challenging might be an application of ab initio molecular dynamics methods to study catalytic reactions over the silica-supported metal oxide systems.

References

1. Sautet P, Delbecq F (2010) Catalysis and surface organometallic chemistry: a view from theory and simulations. Chem Rev 110:1788–1806
2. Handzlik J, Kurleto K (2013) Theoretical investigations of heterogeneous olefin metathesis catalysts. Curr Org Chem 17:2796–2813
3. Handzlik J, Ogonowski J (2012) Structure of isolated molybdenum(VI) and molybdenum(IV) oxide species on silica: periodic and cluster DFT studies. J Phys Chem C 116:5571–5584
4. Handzlik J, Grybos R, Tielens F (2013) Structure of monomeric chromium(VI) oxide species supported on silica: periodic and cluster DFT studies. J Phys Chem C 117:8138–8149
5. Gierada M, Michorczyk P, Tielens F, Handzlik J (2016) Reduction of chromia-silica catalysts: a molecular picture. J Catal 340:122–135
6. Fong A, Yuan Y, Ivry SL, Scott SL, Peters B (2015) Computational kinetic discrimination of ethylene polymerization mechanisms for the Phillips (Cr/SiO$_2$) catalyst. ACS Catal 5:3360–3374
7. Guesmi H, Tielens F (2012) Chromium oxide species supported on silica: a representative periodic DFT model. J Phys Chem C 116:994–1001
8. Guesmi H, Grybos R, Handzlik J, Tielens F (2014) Characterization of molybdenum monomeric oxide species supported on hydroxylated silica: a DFT study. Phys Chem Chem Phys 16:18253–18260
9. Guesmi H, Grybos R, Handzlik J, Tielens F (2016) Characterization of tungsten monomeric oxide species supported on hydroxylated silica; a DFT study. RSC Adv 6:39424–39432
10. Floryan L, Borosy AP, Núñez-Zarur F, Comas-Vives A, Copéret C (2017) Strain effect and dual initiation pathway in Cr^{III}/SiO$_2$ polymerization catalysts from amorphous periodic models. J Catal 346:50–56
11. Dapprich S, Komáromi I, Byun KS, Morokuma K, Frisch MJ (1999) A new ONIOM implementation in Gaussian98. Part I. The calculation of energies, gradients, vibrational frequencies and electric field derivatives. J Mol Struct THEOCHEM 461–462:1–21

12. Ugliengo P, Sodupe M, Musso F, Bush IJ, Orlando R, Dovesi R (2008) Realistic models of hydroxylated amorphous silica surfaces and MCM-41 mesoporous material simulated by large-scale periodic B3LYP calculations. Adv Mater 20:4579–4583

13. Tielens F, Gervais C, Lambert JF, Mauri F, Costa D (2008) Ab initio study of the hydroxylated surface of amorphous silica: a representative model. Chem Mater 20:3336–3344

14. Ewing CS, Bhavsar S, Veser G, McCarthy JJ, Johnson JK (2014) Accurate amorphous silica surface models from first-principles thermodynamics of surface dehydroxylation. Langmuir 30:5133–5141

15. Comas-Vives A (2016) Amorphous SiO_2 surface models: energetics of the dehydroxylation process, strain, ab initio atomistic thermodynamics and IR spectroscopic signatures. Phys Chem Chem Phys 18:7475–7482

16. Gierada M, Petit I, Handzlik J, Tielens F (2016) Hydration in silica based mesoporous materials: a DFT model. Phys Chem Chem Phys 18:32962–32972

17. McDaniel MP (2010) A review of the Phillips supported chromium catalyst and its commercial use for ethylene polymerization. In: Advances in Catalysis, vol. 53, pp. 123–606

18. McDaniel M (2017) Manipulating polymerization chemistry of Cr/silica catalysts through calcination. Appl Catal A Gen 542:392–410

19. Groppo E, Lamberti C, Bordiga S, Spoto G, Zecchina A (2005) The structure of active centers and the ethylene polymerization mechanism on the Cr/SiO_2 catalyst: a frontier for the characterization methods. Chem Rev 105:115–183

20. Weckhuysen BM, Wachs IE, Schoonheydt RA (1996) Surface chemistry and spectroscopy of chromium in inorganic oxides. Chem Rev 96:3327–3349

21. Hakuli A, Harlin ME, Backman LB, Krause AOI (1999) Dehydrogenation of i-butane on CrO_x/SiO_2 catalysts. J Catal 184:349–356

22. Ramani NC, Sullivan DL, Ekerdt JG, Jehng J-M, Wachs IE (1998) Selective oxidation of 1-butene over silica-supported Cr(VI), Mo(VI), and W(VI) oxides. J Catal 176:143–154

23. Cherian M, Rao MS, Hirt AM, Wachs IE, Deo G (2002) Oxidative dehydrogenation of propane over supported chromia catalysts: influence of oxide supports and chromia loading. J Catal 211:482–495

24. Michorczyk P, Pietrzyk P, Ogonowski J (2012) Preparation and characterization of SBA-1-supported chromium oxide catalysts for CO_2 assisted dehydrogenation of propane. Microporous Mesoporous Mater 161:56–66

25. Botavina MA, Agafonov YA, Gaidai NA, Groppo E, Cortés Corberán V, Lapidus AL, Martra G (2016) Towards efficient catalysts for the oxidative dehydrogenation of propane in the presence of CO_2: Cr/SiO_2 systems prepared by direct hydrothermal synthesis. Catal Sci Technol 6:840–850

26. Kim DS, Tatibouet J-M, Wachs IE (1992) Surface structure and reactivity of CrO_3/SiO_2 catalysts. J Catal 136:209–221

27. Jehng J-M, Hu H, Gao X, Wachs IE (1996) The dynamic states of silica-supported metal oxide catalysts during methanol oxidation. Catal Today 28:335–350

28. Liotta LF, Venezia AM, Pantaleo G, Deganello G, Gruttadauria M, Noto R (2004) Chromia on silica and zirconia oxides as recyclable oxidizing system: structural and surface characterization of the active chromium species for oxidation reaction. Catal Today 91–92:231–236

29. Dines TJ, Inglis S (2003) Raman spectroscopic study of supported chromium(VI) oxide catalysts. Phys Chem Chem Phys 5:1320–1328

30. Groppo E, Damin A, Bonino F, Zecchina A, Bordiga S, Lamberti C (2005) New strategies in the Raman study of the Cr/SiO_2 Phillips catalyst: observation of molecular adducts on Cr(II) sites. Chem Mater 17:2019–2027

31. Moisii C, Deguns EW, Lita A, Callahan SD, van de Burgt LJ, Magana D, Stiegman AE (2006) Coordination environment and vibrational spectroscopy of Cr(VI) sites supported on amorphous silica. Chem Mater 18:3965–3975

32. Lee EL, Wachs IE (2007) In situ spectroscopic investigation of the molecular and electronic structures of SiO_2 supported surface metal oxides. J Phys Chem C 111:14410–14425

33. Lee EL, Wachs IE (2008) In situ Raman spectroscopy of SiO_2-supported transition metal oxide catalysts: an isotopic $^{18}O-^{16}O$ exchange study. J Phys Chem C 112:6487–6498

34. Chakrabarti A, Wachs IE (2015) The nature of surface CrO_x sites on SiO_2 in different environments. Catal Lett 145:985–994

35. Peek NM, Jeffcoat DB, Moisii C, van de Burgt L, Profeta S, Scott SL, Stiegman AE (2018) Reassessment of the electronic structure of Cr(VI) sites supported on amorphous silica and implications for Cr coordination number. J Phys Chem C 122:4349–4358

36. Moisii C, Jeffcoat D, Peek N, van de Burgt L, Scott SL, Stiegman AE (2018) Do mono-oxo sites exist in silica-supported Cr(VI) materials? Reassessment of the resonance Raman spectra. J Phys Chem C 122:17149–17160

37. Gaspar AB, Martins RL, Schmal M, Dieguez LC (2001) Characterization of Cr^{2+} and ethylene polymerization on Cr/SiO_2 catalysts. J Mol Catal A Chem 169:105–112

38. Groppo E, Damin A, Otero Arean C, Zecchina A (2011) Enhancing the initial rate of polymerisation of the reduced Phillips catalyst by one order of magnitude. Chem Eur J 17:11110–11114

39. Brown C, Krzystek J, Achey R, Lita A, Fu R, Meulenberg RW, Polinski M, Peek N, Wang Y, van de Burgt LJ, Profeta S, Stiegman AE, Scott SL (2015) Mechanism of initiation in the Phillips ethylene polymerization catalyst: redox processes leading to the active site. ACS Catal 5:5574–5583

40. Chakrabarti A, Gierada M, Handzlik J, Wachs IE (2016) Operando molecular spectroscopy during ethylene polymerization by supported CrO_x/SiO_2 catalysts: active sites, reaction intermediates, and structure-activity relationship. Top Catal 59:725–739

41. Barzan C, Piovano A, Braglia L, Martino GA, Lamberti C, Bordiga S, Groppo E (2017) Ligands make the difference! Molecular insights into Cr^{VI}/SiO_2 Phillips catalyst during ethylene polymerization. J Am Chem Soc 139:17064–17073

42. Weckhuysen BM, De Ridder LM, Schoonheydt RA (1993) A quantitative diffuse reflectance spectroscopy study of supported chromium catalysts. J Phys Chem 97:4756–4763

43. Liu B, Nakatani H, Terano M (2002) New aspects of the induction period of ethene polymerization using Phillips CrO_x/SiO_2 catalyst probed by XPS, TPD and EPMA. J Mol Catal A Chem 184:387–398

44. Budnyk A, Damin A, Groppo E, Zecchina A, Bordiga S (2015) Effect of surface hydroxylation on the catalytic activity of a $Cr(II)/SiO_2$ model system of Phillips catalyst. J Catal 324:79–87

45. Weckhuysen BM, De Ridder LM, Grobet PJ, Schoonheydt RA (1995) Redox behavior and dispersion of supported chromium catalysts. J Phys Chem 99:320–326

46. Weckhuysen BM, Schoonheydt RA, Mabbs FE, Collison D (1996) Electron paramagnetic resonance of heterogeneous chromium catalysts. J Chem Soc Faraday Trans 92:2431–2436

47. Brown C, Lita A, Tao Y, Peek N, Crosswhite M, Mileham M, Krzystek J, Achey R, Fu R, Bindra JK, Polinski M, Wang Y, van de Burgt LJ, Jeffcoat D, Profeta S, Stiegman AE, Scott SL (2017) Mechanism of initiation in the Phillips ethylene polymerization catalyst: ethylene activation by Cr(II) and the structure of the resulting active site. ACS Catal 7:7442–7455

48. Espelid Ø, Børve KJ (2001) Theoretical analysis of d-d transitions for the reduced Cr/silica system. Catal Lett 75:49–54

49. Espelid Ø, Børve KJ (2002) Theoretical analysis of CO adsorption on the reduced Cr/silica system. J Catal 205:177–190

50. Damin A, Vitillo JG, Ricchiardi G, Bordiga S, Lamberti C, Groppo E, Zecchina A (2009) Modeling CO and N_2 adsorption at Cr surface species of Phillips catalyst by hybrid density functionals: effect of Hartree-Fock exchange percentage. J Phys Chem A 113:14261–14269

51. Demmelmaier CA, White RE, van Bokhoven JA, Scott SL (2008) Nature of $\equiv SiOCrO_2Cl$ and $(\equiv SiO)_2CrO_2$ sites prepared by grafting CrO_2Cl_2 onto silica. J Phys Chem C 112:6439–6449

52. Demmelmaier CA, White RE, van Bokhoven JA, Scott SL (2009) Evidence for a chromasiloxane ring size effect in Phillips (Cr/SiO_2) polymerization catalysts. J Catal 262:44–56

53. Zhong L, Lee M-Y, Liu Z, Wanglee Y-J, Liu B, Scott SL (2012) Spectroscopic and structural characterization of $Cr(II)/SiO_2$ active site precursors in model Phillips polymerization catalysts. J Catal 293:1–12

54. Handzlik J, Kurleto K (2013) Assessment of density functional methods for thermochemistry of chromium oxo compounds and their application in a study of chromia-silica system. Chem Phys Lett 561–562:87–91

55. Handzlik J (2009) DFT study of molybdena-silica system—a selection of density functionals based on their performance in thermochemistry of molybdenum compounds. Chem Phys Lett 469:140–144

56. Cheng R, Liu X, Fang Y, Terano M, Liu B (2017) High-resolution ^{29}Si CP/MAS solid state NMR spectroscopy and DFT investigation on the role of geminal and single silanols in grafting chromium species over Phillips Cr/silica catalyst. Appl Catal A Gen 543:26–33

57. Zhuravlev LT (2000) The surface chemistry of amorphous silica. Zhuravlev model. Colloids Surfaces A Physicochem Eng Asp 173:1–38

58. Ek S, Root A, Peussa M, Niinistö L (2001) Determination of the hydroxyl group content in silica by thermogravimetry and a comparison with ^{1}H MAS NMR results. Thermochim Acta 379:201–212

59. Lillehaug S, Børve KJ, Sierka M, Sauer J (2004) Catalytic dehydrogenation of ethane over mononuclear Cr(III) surface sites on silica. Part I. C-H activation by σ-bond metathesis. J Phys Org Chem 17:990–1006

60. Lillehaug S, Jensen VR, Børve KJ (2006) Catalytic dehydrogenation of ethane over mononuclear Cr(III)-silica surface sites. Part 2: C-H activation by oxidative addition. J Phys Org Chem 19:25–33

61. Liu Z, Cheng R, He X, Wu X, Liu B (2012) DFT functional benchmarking on the energy splitting of chromium spin states and mechanistic study of acetylene cyclotrimerization over the Phillips Cr(II)/silica catalyst. J Phys Chem A 116:7538–7549

62. Liu Z, Cheng R, He X, Liu B (2013) Reactivity and regioselectivity of methylacetylene cyclotrimerization over the Phillips Cr/silica catalyst: a DFT study. ACS Catal 3:1172–1183

63. Espelid Ø, Børve KJ (2000) Theoretical models of ethylene polymerization over a mononuclear chromium(II)/silica site. J Catal 195:125–139

64. Espelid Ø, Børve KJ (2002) Molecular-level insight into Cr/silica Phillips-type catalysts: polymerization-active mononuclear chromium sites. J Catal 205:366–374

65. Espelid Ø, Børve KJ (2002) Molecular-level insight into Cr/silica Phillips-type catalysts: polymerization-active dinuclear chromium sites. J Catal 206:331–338

66. Potter KC, Beckerle CW, Jentoft FC, Schwerdtfeger E, McDaniel MP (2016) Reduction of the Phillips catalyst by various olefins: stoichiometry, thermochemistry, reaction products and polymerization activity. J Catal 344:657–668

67. Zhong L, Liu Z, Cheng R, Tang S, Qiu P, He X, Terano M, Liu B (2012) Active site transformation during the induction period of ethylene polymerization over the Phillips CrO$_x$/SiO$_2$ catalyst. ChemCatChem 4:872–881

68. Liu B, Nakatani H, Terano M (2003) Mechanistic implications of the unprecedented transformations of ethene into propene and butene over Phillips CrO$_x$/SiO$_2$ catalyst during induction period. J Mol Catal A: Chem 201:189–197

69. Conley MP, Delley MF, Siddiqi G, Lapadula G, Norsic S, Monteil V, Safonova OV, Copéret C (2014) Polymerization of ethylene by silica-supported dinuclear Cr^{III} sites through an initiation step involving C-H bond activation. Angew Chem Int Ed 53:1872–1876

70. Conley MP, Delley MF, Núñez-Zarur F, Comas-Vives A, Copéret C (2015) Heterolytic activation of C-H bonds on Cr^{III}-O surface sites is a key step in catalytic polymerization of ethylene and dehydrogenation of propane. Inorg Chem 54:5065–5078

71. Gierada M, Handzlik J (2017) Active sites formation and their transformations during ethylene polymerization by the Phillips CrO$_x$/SiO$_2$ catalyst. J Catal 352:314–328

72. Delley MF, Praveen CS, Borosy AP, Núñez-Zarur F, Comas-Vives A, Copéret C (2017) Olefin polymerization on Cr(III)/SiO$_2$: mechanistic insights from the differences in reactivity between ethene and propene. J Catal 354:223–230

73. Fong A, Peters B, Scott SL (2016) One-electron-redox activation of the reduced Phillips polymerization catalyst, via alkylchromium(IV) homolysis: a computational assessment. ACS Catal 6:6073–6085

74. Kissin YV, Brandolini AJ (2008) Chemistry of olefin polymerization reactions with chromium-based catalysts. J Polym Sci Part A Polym Chem 46:5330–5347
75. Fong A, Vandervelden C, Scott SL, Peters B (2018) Computational support for Phillips catalyst initiation via Cr-C bond homolysis in a chromacyclopentane site. ACS Catal 8:1728–1733
76. Gierada M, Handzlik J (2018) Computational insights into reduction of the Phillips CrO_x/SiO_2 catalyst by ethylene and CO. J Catal 359:261–271
77. Shelimov BN, Elev IV, Kazansky VB (1986) Use of photoreduction for activation of silica-molybdena catalysts for propylene metathesis: comparison with thermal reduction. J Catal 98:70–81
78. Vikulov KA, Elev IV, Shelimov BN, Kazansky VB (1989) IR and UV-vis spectroscopic studies of the stable $Mo=CH_2$ carbene complexes over photoreduced silica-molybdena catalysts with chemisorbed cyclopropane, and their role in olefin metathesis reactions. J Mol Catal 55:126–145
79. Zhang B, Liu N, Lin Q, Jin D (1991) The effects of Mo oxidation states on olefin metathesis. J Mol Catal 65:15–28
80. Handzlik J, Ogonowski J, Stoch J, Mikołajczyk M, Michorczyk P (2006) Properties and metathesis activity of molybdena-alumina, molybdena-silica-alumina and molybdena-silica catalysts—a comparative study. Appl Catal A Gen 312:213–219
81. Balcar H, Mishra D, Marceau E, Carrier X, Žilková N, Bastl Z (2009) Molybdenum oxide catalysts for metathesis of higher 1-alkenes via supporting MoO_2(acetylacetonate)$_2$ and MoO_2(glycolate)$_2$ on SBA-15 mesoporous molecular sieves. Appl Catal A Gen 359:129–135
82. Amakawa K, Wrabetz S, Kröhnert J, Tzolova-Müller G, Schlögl R, Trunschke A (2012) In situ generation of active sites in olefin metathesis. J Am Chem Soc 134:11462–11473
83. Amakawa K, Kröhnert J, Wrabetz S, Frank B, Hemmann F, Jäger C, Schlögl R, Trunschke A (2015) Active sites in olefin metathesis over supported molybdena catalysts. ChemCatChem 7:4059–4065
84. Lwin S, Wachs IE (2014) Olefin metathesis by supported metal oxide catalysts. ACS Catal 4:2505–2520
85. Ding K, Gulec A, Johnson AM, Drake TL, Wu W, Lin Y, Weitz E, Marks LD, Stair PC (2016) Highly efficient activation, regeneration, and active site identification of oxide-based olefin metathesis catalysts. ACS Catal 6:5740–5746
86. Banares MA, Fierro JLG, Moffat JB (1993) The partial oxidation of methane on MoO_3/SiO_2 catalysts: influence of the molybdenum content and type of oxidant. J Catal 142:406–417
87. Ohler N, Bell AT (2005) Selective oxidation of methane over MoO_x/SiO_2: isolation of the kinetics of reactions occurring in the gas phase and on the surfaces of SiO_2 and MoO_x. J Catal 231:115–130
88. Ohler N, Bell AT (2006) Study of the elementary processes involved in the selective oxidation of methane over MoO_x/SiO_2. J Phys Chem B 110:2700–2709
89. Thielemann JP, Hess C (2012) Structure of silica-supported molybdenum oxide studied by in situ spectroscopy under reactive and non-reactive conditions. J Catal 288:124–126
90. Thielemann JP, Hess C (2013) Monitoring silica supported molybdenum oxide catalysts at work: a Raman spectroscopic study. ChemPhysChem 14:441–447
91. Ono T, Anpo M, Kubokawa Y (1986) Catalytic activity and structure of MoO_3 highly dispersed on SiO_2. J Phys Chem 90:4780–4784
92. Banares MA, Hu HC, Wachs IE (1994) Molybdena on silica catalysts: role of preparation methods on the structure-selectivity properties for the oxidation of methanol. J Catal 150:407–420
93. Zhang W, Desikan A, Oyama ST (1995) Effect of support in ethanol oxidation on molybdenum oxide. J Phys Chem 99:14468–14476
94. Biermann JJP, Janssen FJJG, Ross JRH (1992) Nitrogen containing species as intermediates in the oxidation of ammonia over silica supported molybdena catalysts. Appl Catal A Gen 86:165–179
95. Hu H, Wachs IE, Bare SR (1995) Surface structures of supported molybdenum oxide catalysts: characterization by Raman and Mo L^3-edge XANES. J Phys Chem 99:10897–10910

96. Takenaka S, Tanaka T, Funabiki T, Yoshida S (1998) Structures of molybdenum species in silica-supported molybdenum oxide and alkali-ion-modified silica-supported molybdenum oxide. J Phys Chem B 102:2960–2969

97. Radhakrishnan R, Reed C, Oyama ST, Seman M, Kondo JN, Domen K, Ohminami Y, Asakura K (2001) Variability in the structure of supported MoO_3 catalysts: studies using Raman and X-ray absorption spectroscopy with ab initio calculations. J Phys Chem B 105:8519–8530

98. Ohler N, Bell AT (2005) A study of the redox properties of MoO_x/SiO_2. J Phys Chem B 109:23419–23429

99. Tian H, Roberts CA, Wachs IE (2010) Molecular structural determination of molybdena in different environments: aqueous solutions, bulk mixed oxides, and supported MoO_3 catalysts. J Phys Chem C 114:14110–14120

100. Wachs IE, Roberts CA (2010) Monitoring surface metal oxide catalytic active sites with Raman spectroscopy. Chem Soc Rev 39:5002–5017

101. Guo CS, Hermann K, Hävecker M, Thielemann JP, Kube P, Gregoriades LJ, Trunschke A, Sauer J, Schlögl R (2011) Structural analysis of silica-supported molybdena based on X-ray spectroscopy: quantum theory and experiment. J Phys Chem C 115:15449–15458

102. Thielemann JP, Kröhnert J, Hess C (2010) Nitric oxide adsorption and oxidation on SBA-15 supported molybdenum oxide: a transmission IR study. J Phys Chem C 114:17092–17098

103. Thielemann JP, Ressler T, Walter A, Tzolova-Müller G, Hess C (2011) Structure of molybdenum oxide supported on silica SBA-15 studied by Raman, UV-Vis and X-ray absorption spectroscopy. Appl Catal A Gen 399:28–34

104. Amakawa K, Sun L, Guo C, Hävecker M, Kube P, Wachs IE, Lwin S, Frenkel AI, Patlolla A, Hermann K, Schlögl R, Trunschke A (2013) How strain affects the reactivity of surface metal oxide catalysts. Angew Chem Int Ed 52:13553–13557

105. Louis C, Che M (1987) EPR investigation of the coordination sphere of Mo^{5+} ions on thermally reduced silica-supported molybdenum catalysts prepared by the grafting method. J Phys Chem 91:2875–2883

106. Chempath S, Zhang Y, Bell AT (2007) DFT studies of the structure and vibrational spectra of isolated molybdena species supported on silica. J Phys Chem C 111:1291–1298

107. Gregoriades LJ, Döbler J, Sauer J (2010) Oxidation of methanol to formaldehyde on silica-supported molybdena: density functional theory study on models of mononuclear sites. J Phys Chem C 114:2967–2979

108. Chempath S, Bell AT (2007) A DFT study of the mechanism and kinetics of methane oxidation to formaldehyde occurring on silica-supported molybdena. J Catal 247:119–126

109. Handzlik J (2005) Metathesis activity and properties of Mo-alkylidene sites differently located on silica. A density functional theory study. J Phys Chem B 109:20794–20804

110. Handzlik J (2007) Application of the ONIOM (QM/QM) method in the study of molybdena–silica system active in olefin metathesis. Int J Quantum Chem 107:2111–2119

111. Handzlik J (2007) Theoretical investigations of isolated Mo(VI) and Mo(IV) centers of a molybdena-silica catalyst for olefin metathesis. J Phys Chem C 111:9337–9348

112. Handzlik J, Ogonowski J (2002) DFT study of ethene metathesis proceeding on monomeric Mo^{VI} centres of MoO_3/Al_2O_3 catalyst. The role of the molybdacyclobutane intermediate. J Mol Catal A: Chem 184:371–377

113. Handzlik J (2004) Metathesis activity of monomeric Mo-methylidene centres on (1 0 0) and (1 1 0)C surfaces of γ-Al_2O_3—a comparative DFT study. Surf Sci 562:101–112

114. Handzlik J, Ogonowski J, Tokarz-Sobieraj R (2005) Dependence of metathesis activity of Mo-methylidene sites on their location on (1 0 0) γ-Al_2O_3—a theoretical study. Catal Today 101:163–173

115. Handzlik J (2007) Properties and metathesis activity of monomeric and dimeric Mo centres variously located on γ-alumina—a DFT study. Surf Sci 601:2054–2065

116. Handzlik J, Sautet P (2008) Active sites of olefin metathesis on molybdena-alumina system: a periodic DFT study. J Catal 256:1–14

117. Handzlik J, Czernecki M, Shiga A, Śliwa P (2012) Paired interacting orbitals (PIO) study of Mo/SiO_2 and Mo/HZSM-5 catalysts for olefin metathesis. Comput Theor Chem 991:174–181

118. Goldsmith BR, Sanderson ED, Bean D, Peters B (2013) Isolated catalyst sites on amorphous supports: a systematic algorithm for understanding heterogeneities in structure and reactivity. J Chem Phys 138:204105
119. Ewing CS, Bagusetty A, Patriarca EG, Lambrecht DS, Veser G, Johnson JK (2016) Impact of support interactions for single-atom molybdenum catalysts on amorphous silica. Ind Eng Chem Res 55:12350–12357
120. Mol JC (2004) Industrial applications of olefin metathesis. J Mol Catal A Chem 213:39–45
121. Lwin S, Li Y, Frenkel AI, Wachs IE (2016) Nature of WO_x sites on SiO_2 and their molecular structure-reactivity/selectivity relationships for propylene metathesis. ACS Catal 6:3061–3071
122. Lwin S, Wachs IE (2017) Catalyst activation and kinetics for propylene metathesis by supported WO_x/SiO_2 catalysts. ACS Catal 7:573–580
123. Howell JG, Li Y-P, Bell AT (2016) Propene metathesis over supported tungsten oxide catalysts: a study of active site formation. ACS Catal 6:7728–7738
124. de Lucas A, Valverde JL, Cañizares P, Rodriguez L (1999) Partial oxidation of methane to formaldehyde over W/SiO_2 catalysts. Appl Catal A Gen 184:143–152
125. Adam F, Iqbal A (2011) The liquid phase oxidation of styrene with tungsten modified silica as a catalyst. Chem Eng J 171:1379–1386
126. Liu G, Wang X, Wang X, Han H, Li C (2012) Photocatalytic H_2 and O_2 evolution over tungsten oxide dispersed on silica. J Catal 293:61–66
127. Ross-Medgaarden EI, Wachs IE (2007) Structural determination of bulk and surface tungsten oxides with UV-vis diffuse reflectance spectroscopy and Raman spectroscopy. J Phys Chem C 111:15089–15099
128. Chauvin J, Thomas K, Clet G, Houalla M (2015) Comparative influence of surface tungstate species and bulk amorphous WO_3 particles on the acidity and catalytic activity of tungsten oxide supported on silica. J Phys Chem C 119:12345–12355